



King's Research Portal

[Link to publication record in King's Research Portal](#)

Citation for published version (APA):

Robson, D. T., Annibale, A., & Baas, A. C. W. (2022). Reproducing size distributions of swarms of barchan dunes on Mars and Earth using a mean-field model. *PHYSICA A*, [128042].

Citing this paper

Please note that where the full-text provided on King's Research Portal is the Author Accepted Manuscript or Post-Print version this may differ from the final Published version. If citing, it is advised that you check and use the publisher's definitive version for pagination, volume/issue, and date of publication details. And where the final published version is provided on the Research Portal, if citing you are again advised to check the publisher's website for any subsequent corrections.

General rights

Copyright and moral rights for the publications made accessible in the Research Portal are retained by the authors and/or other copyright owners and it is a condition of accessing publications that users recognize and abide by the legal requirements associated with these rights.

- Users may download and print one copy of any publication from the Research Portal for the purpose of private study or research.
- You may not further distribute the material or use it for any profit-making activity or commercial gain
- You may freely distribute the URL identifying the publication in the Research Portal

Take down policy

If you believe that this document breaches copyright please contact librarypure@kcl.ac.uk providing details, and we will remove access to the work immediately and investigate your claim.

Reproducing size distributions of swarms of barchan dunes on Mars and Earth using a mean-field model

Dominic T Robson^a, Alessia Annibale^b, Andreas CW Baas^a

^a*King's College London Department of Geography, King's College London, Bush House, North East Wing, 40 Aldwych, London, WC2B 4BG, UK*

^b*King's College London Department of Mathematics, King's College London, Strand Building, Strand Campus, Strand, London, WC2R 2LS, UK*

Abstract

We apply a mean-field model of interactions between migrating barchan dunes, the CAFE model, which includes calving, aggregation, fragmentation, and mass-exchange, yielding a steady-state size distribution that can be resolved for different choices of interaction parameters. The CAFE model is applied to empirically measured distributions of dune sizes in two barchan swarms on Mars, three swarms in Morocco, and one in Mauritania, each containing 1000 bedforms, comparing the observed size distributions to the steady-states of the CAFE model. We find that the distributions in the Martian swarm are very similar to the swarm measured in Mauritania, suggesting that the two very different planetary environments however share similar dune interaction dynamics. Optimisation of the model parameters of three specific configurations of the CAFE model shows that the fit of the theoretical steady-state is often superior to the typically assumed log-normal. In all cases, the optimised parameters indicate that mass-exchange is the most frequent type of interaction. Calving is found to occur rarely in most of the swarms, with a highest rate of only 9% of events, showing that interactions between multiple dunes rather than spontaneous calving are the driver of barchan size distributions. Finally, the implementation of interaction parameters derived from 3D simulations of dune-pair collisions indicates that sand flux between dunes is more important in producing the size distributions of the Moroccan swarms than of those in Mauritania and on Mars.

1. Introduction

Barchan dunes are a class of aeolian bedform that are found in many areas on Mars and Earth under unidirectional wind regimes and relatively low sediment supply conditions [1, 2]. Under such a near-constant wind direction, the dunes form into their striking crescentic shape with steep slip-faces resulting from avalanching [3]. Properties of individual barchans, such as relationships between migration rate and size or between the various morphometric parameters, are well-known [3, 4, 5, 6, 7, 8, 9, 10, 11]. However, simulations have shown that the size of isolated barchans is not stable but should rather grow indefinitely or shrink and vanish [12, 13, 14, 15, 16]. In reality, barchans are not found as isolated dunes but in vast collections, known as swarms, which can contain tens of thousands of dunes [14, 4, 17, 18]. By now it has been established that within these swarms the size distribution of barchans is homogeneous in the direction of the wind. This homogeneity contrasts with the instability observed in simulations where one would expect that the average size should increase linearly with downwind distance [18]. The discrepancy between

simulated and observed behaviours suggests that the apparent stability of barchans in swarms is an emergent property resulting from the interactions of the dunes. There are two main types of interaction that are thought to be important in barchan swarms: calving, where a large dune breaks into two smaller ones [4, 19, 20], and collisions [17, 18, 21, 22, 23].

Owing to the long timescales over which these processes occur in real-world dune fields, studies of these interactions are typically performed using computer simulations [17, 12, 22, 24] or in water-tanks in laboratories [21, 25, 26]. However, it is not clear that the results of simulations and water-tanks experiments are entirely scalable to the real world. In this work, we explore an alternative approach whereby the steady-state distribution of a mean-field model is fit to the size distributions of real-world barchan swarms by adjusting the rules for the different interactions. Mean-field models have previously been used to study barchan swarms [17, 23], however, these models did not feature adjustable collision rules and did not include all of the types of interaction known to occur in these systems.

We recently developed a generalised mean-field model which can be applied to understand the steady-state distributions of collections interacting bodies [27]. The model unites continuous aggregation-fragmentation and asset-exchange models and, as such, can include any $n \rightarrow m$ process in which an extrinsic quantity is conserved. Despite the generality of the processes permitted in the model, it is possible to analytically derive the integer moments of the steady-state distribution of the conserved quantity as well as find a self-consistency equation for the steady-state distribution itself. Although any processes can be included, for this work we limited ourselves to only those processes which have been observed in experiments and simulations. We compared the steady-state outputs of this modelling to real-world size distributions which we measured for several locations on both Mars and Earth.

In section 2 we provide a description of the mean-field model and tailor the results of the generalised model [27] to the processes which are relevant to barchan swarms. We then describe, in section 3, the methods by which we measured the sizes of the real-world barchans and the locations of the swarms we studied. In section 4 we show the distributions we observed for the swarms, describe how we then optimised the model parameters to reproduce these, and show the results of the optimisation, reserving discussion of the physical relevance of these findings and how the work may be improved to sections 5 and 6.

2. Mean-field modelling

Mean-field models are useful tools in studying the global properties of large populations. The model we apply in this work is a specific implementation of the general mean-field model which we have described in [27].

2.1. Interactions

We consider a system comprising $N(t)$ interacting particles (dunes) at time t . The dunes are characterised by their volume, a continuous quantity distributed according to a volume probability density function (pdf) $p(v, t)$. Note here that, since the bulk density will be approximately the

same in all the barchans within a field, volume is equivalent to mass.

In the general model [27] we allowed for any $n \rightarrow m$ interactions in which volume is conserved. Here we limit ourselves to only those interactions which are known to be relevant in barchan swarms, focusing on four interactions:

- *Calving* - a $1 \rightarrow 2$ process where a dune spontaneously breaks apart.
- *Aggregation* - a $2 \rightarrow 1$ process where two dunes merge together.
- *Fragmentation* - a $2 \rightarrow 3$ process where two dunes break into three.
- *Exchange* - a $2 \rightarrow 2$ process where volume is transferred between the dunes.

Calving is thought to occur in barchan swarms due to changes in the wind or events such as storms which can destabilise larger dunes resulting in a smaller barchan breaking off of the flank [4, 28]. Barchans have been observed to aggregate (typically termed merging) in real-world fields [5] as well as in simulations [17, 12, 18] and water-tank experiments [21].

Fragmentation interactions have also been observed in various settings [17, 12, 18, 21, 19] with several different types of fragmentation (e.g. “fragmentation-chasing” and “fragmentation-exchange” [21]) having been described. In our model, we include only one $2 \rightarrow 3$ process as it is not clear if the different types of fragmentation interaction produce significantly different outputs. We would also like to note that, in the barchan literature, “calving” sometimes also refers to a $2 \rightarrow 3$ process [4, 19] however in this work we will only use the term to describe the spontaneous $1 \rightarrow 2$ process.

Finally, the exchange process has also been observed in nature [29], simulations [17, 12, 18, 30], and experiments [21].

Since the model we are describing in this work features only these four interactions we will refer to it as the Calving, Aggregation, Fragmentation, and Exchange (CAFE) model.

For the CAFE model we assume that all four interactions conserve volume so that the total volume of all the dunes in the system is conserved. In real-world systems, we believe that collisions ought to be at least approximately conservative, and this assumption is in line with previous agent-based and mean-field modelling of barchan fields [17, 18, 23, 20, 22, 31].

2.2. Output channels and interaction rules

In [27] we introduce the concept of *output channels* (OCs) which is pivotal in our derivations. OCs give expressions, based on the choice of *interaction rules*, for the individual outputs of all the possible types of interaction. There are two outputs of calving, one of aggregation, three of fragmentation, and two of exchange so we have eight OCs in our model here.

Consider a dune of volume v_a calving to yield dunes with volumes v_1 and v_2 these are OC1 and OC2. Volume conservation tells us that $v_1 + v_2 = v_a$ but we need one additional piece of information to determine the two volumes. This additional piece of information is the interaction rule for the

calving process, in this case, the ratio between the two output dunes, r_c (always taking the smaller dune in the numerator). To derive analytical results in [27] we only consider random interactions. We make the same choice again here defining our interaction rule as a probability distribution, $p_c(r_c)$, which is the distribution from which the stochastic variable $r_c = v_2/v_1$ is drawn. We now have enough information to define the two OCs associated with calving

$$v_1 = \frac{v_a}{1+r_c} \quad \text{and} \quad v_2 = \frac{v_a r_c}{1+r_c}. \quad (1)$$

For the remainder of the interactions we consider inputs v_a and v_b and introducing additional stochastic variables r_{f_1} , r_{f_2} , and r_e drawn from distributions $p_{f_1}(r_{f_1})$, $p_{f_2}(r_{f_2})$, and $p_e(r_e)$. The OCs are then defined as for aggregation,

$$v_3 = v_a + v_b, \quad (2)$$

for fragmentation,

$$v_4 = \frac{v_a + v_b}{1+r_{f_1}}, \quad (3)$$

$$v_5 = \frac{(v_a + v_b)r_{f_1}}{(1+r_{f_1})(1+r_{f_2})}, \quad (4)$$

$$v_6 = \frac{(v_a + v_b)r_{f_1}r_{f_2}}{(1+r_{f_1})(1+r_{f_2})}, \quad (5)$$

and for exchange collisions

$$v_7 = \frac{v_a + v_b}{1+r_e}, \quad (6)$$

$$v_8 = \frac{(v_a + v_b)r_e}{1+r_e}. \quad (7)$$

2.3. Rates and channel probabilities

Evaluating the time evolution of $p(v, t)$ requires understanding how often the OCs create a dune of volume v . We have already defined the OCs but have yet to discuss the rate at which the interactions occur.

Since we are considering a mean-field model, in any n -body interaction, all combinations of n -dunes must be equally likely to be involved. At time t there are $\binom{N(t)}{n}$ such combinations and therefore the rate at which n -body interactions occur is proportional to $\binom{N(t)}{n}$. We refer to the proportionality constants as *rate coefficients* which we label α_c , α_a , α_f , and α_e for calving, aggregation, fragmentation, and exchange respectively. OC1 and OC2 are outputs of calving, a one-body interaction, while the other OCs are results of two-body interactions. We can now write the channel probabilities p_i which are given as the rate of a particular channel divided by the total rates of all channels α_{out} [27]

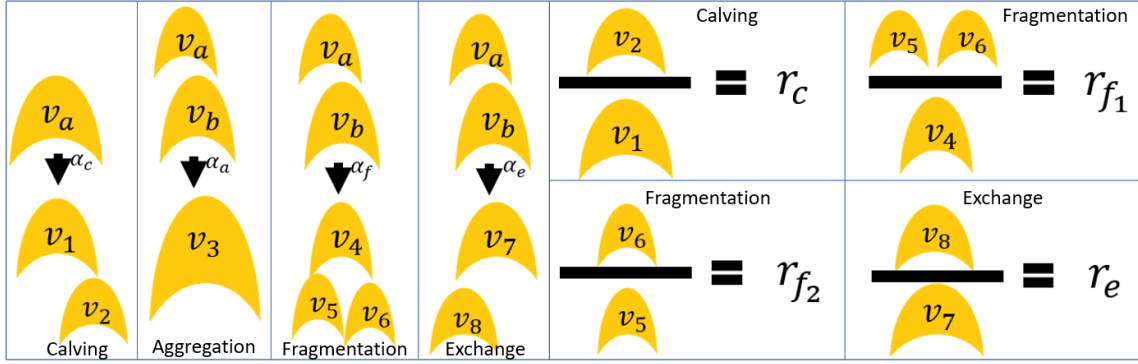


Figure 1: The four processes (left to right: calving, aggregation, fragmentation, and exchange), eight output channels of the CAFE model (v_1, \dots, v_8), and the definitions of the stochastic variables (r_c, r_{f_1}, r_{f_2} , and r_e) which define the interaction rules. The rate coefficients $\alpha_c, \alpha_a, \alpha_f, \alpha_e$ of the four processes are also shown.

$$p_1 = p_2 = \frac{\alpha_c}{\alpha_{out}} N(t), \quad (8)$$

$$p_3 = \frac{\alpha_a}{2\alpha_{out}} N(t)(N(t) - 1), \quad (9)$$

$$p_4 = p_5 = p_6 = \frac{\alpha_f}{2\alpha_{out}} N(t)(N(t) - 1), \quad (10)$$

$$p_7 = p_8 = \frac{\alpha_e}{2\alpha_{out}} N(t)(N(t) - 1), \quad (11)$$

where

$$\alpha_{out} = 2\alpha_c N(t) + \frac{\alpha_a + 3\alpha_f + 2\alpha_e}{2} N(t)(N(t) - 1). \quad (12)$$

Channel probabilities represent the fractions of dunes in the population that were generated through each OC, while α_{out} gives the total rate at which outputs are generated. Together with the definitions of the output channels, we have now completely defined the CAFE model. The key aspects of the model are shown pictorially in figure 1.

The free parameters of the model are the rate coefficients, the distributions of the stochastic variables, and the total volume of all the dunes. If we know the steady-state population size, N_s , not all of the rate coefficients are free parameters since the steady population size requires a balance between the additive interactions (fragmentation and calving) and the reductive interactions (aggregation). In the CAFE model, the steady-state population size is

$$N_s = 1 + \frac{2\alpha_c}{\alpha_a - \alpha_f}, \quad (13)$$

which we use as a constraint on α_a .

2.4. Master equation and steady-state probability density function

Having completely defined the model we can now insert all of the terms into the general equations we derived in [27]. The evolution of $p(v, t)$ is determined by the balance between the creation of dunes of volume v through the output channels, and the loss of dunes of volume v due to such dunes being involved in interactions. The balance of the loss and gain terms combine to give a master equation for the time-derivative of $p(v, t)$

$$\dot{p}(v, t) = \frac{\alpha_{out}}{N(t)} (p_{gain}(v, t) - p(v, t)), \quad (14)$$

where

$$p_{gain}(v, t) = \langle \delta(v_i(v_a, v_b, r_c, r_{f_1}, r_{f_2}, r_e) - v) \rangle_{i, v_a, v_b, r_c, r_{f_1}, r_{f_2}, r_e}, \quad (15)$$

with $\delta(x)$ denoting the Dirac δ -function and $\langle \cdot \rangle_x$ the average over the distribution of x . Averaging over the OCs is done using the channel probabilities, p_i . Note that $p_{gain}(v, t)$ involves averaging over the distributions of v_a and v_b which are the volume pdf $p(v, t)$ if we assume that the population is large enough such that their distributions can be thought of as independent.

It is trivial to write an expression for the steady-state volume pdf $p_s(v)$ by setting $\dot{p}(v, t) = 0$ in equation (14) which gives

$$p_s(v) = \langle \delta(v_i(v_a, v_b, r_c, r_{f_1}, r_{f_2}, r_e) - v) \rangle_{i, v_a, v_b, r_c, r_{f_1}, r_{f_2}, r_e}^{(s)}, \quad (16)$$

where we have used the superscript (s) to denote that the distributions of v_a and v_b on the right hand side of (16) are also the steady-state distribution $p_s(v)$. This is a self-consistency equation as the steady-state pdf appears on both sides. The form of the self-consistency equation means, however, that it can easily be solved using a population dynamics algorithm [27, 32, 33].

2.5. Steady-state moments

As well as a self-consistency equation for the steady-state pdf, it is also possible to write exact expressions for the steady-state moments [27]. As we have already stated, the total volume of dunes in the system is a free parameter, which, when divided by the steady-state population size N_s , gives the mean volume $\langle v \rangle_s$, where the subscript, s , denotes that this is in the steady-state. The higher integer moments $\langle v^\ell \rangle_s$ for $\ell \geq 2$ can then be calculated iteratively [27] using

$$\langle v^\ell \rangle_s = \frac{K_\ell}{Z_\ell} \sum_{j=1}^{\ell-1} \binom{\ell}{j} \langle v^j \rangle_s \langle v^{\ell-j} \rangle_s, \quad (17)$$

where

$$K_\ell = \frac{N_s(N_s - 1)}{2\alpha_{out}^{(s)}} \left(\alpha_a + \alpha_f \left\langle \frac{1 + r_{f_1}^\ell \frac{1+r_{f_2}^\ell}{(1+r_{f_2})^\ell}}{(1+r_{f_1})^\ell} \right\rangle_{r_{f_1}, r_{f_2}} + \alpha_e \left\langle \frac{1 + r_e^\ell}{(1+r_e)^\ell} \right\rangle_{r_e} \right) \quad (18)$$

and where

$$Z_\ell = 1 - 2K_\ell - \frac{\alpha_e N_s}{\alpha_{out}^{(s)}} \left\langle \frac{1 + r_c^\ell}{(1+r_c)^\ell} \right\rangle_{r_c}. \quad (19)$$

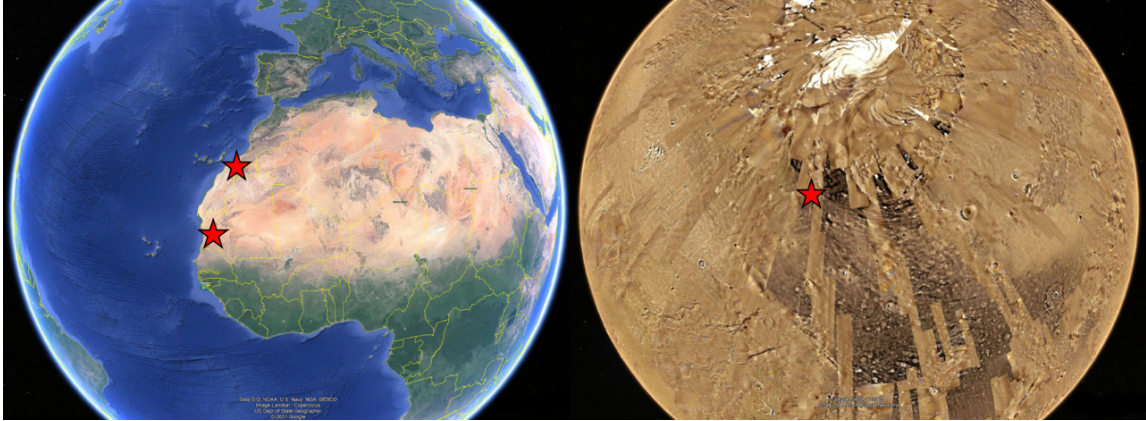


Figure 2: The locations of the zones of study on Earth and on Mars are marked as stars. On Earth, the more northerly star covers the locations of the three zones in Tarfaya Province while the more southerly marker covers the field in Mauritania. Image courtesy of Google Earth.

3. Measuring size distributions of real-world barchan swarms

In this section, we describe the locations of the real-world barchan swarms which we have measured and the method we used for extracting the sizes of the dunes.

3.1. Zones of study

A swarm of barchan dunes is a two-dimensional many-body system in which the bedforms all migrate in approximately the same direction, that of the dominant wind. Typically, mean-field models such as ours do not apply to such low-dimensional systems because they rely upon an assumption that the systems are well-mixed [34]. However, large swarms of barchans are thought to be homogeneous in the direction of the wind [4, 18]. As such, one can effectively treat a zone within the bulk of a large swarm as having periodic boundaries, so that the assumption of sufficient mixing is valid within the zone. Support for this claim can be found in [23] where size distributions in an agent-based model with periodic boundaries were approximately replicated using mean-field models.

Although barchan swarms occur at many locations on Earth [2] and Mars [1], in most of these locations the populations of barchans are limited in number and typically situated between different classes of bedforms such as barchanoid ridges, meaning that the assumption of periodic boundaries may not hold.

We limit ourselves to swarms in which we could define zones of ~ 1000 barchans such that the dunes immediately upwind of the zone appeared qualitatively similar to those within the zone. For this study, we selected six zones: three located approximately 17km west of El Hagounia, Tarfaya Province in a large field which extends southward from the northern Atlantic coast of Morocco; one around 60km south of Akjoujt, Mauritania in a field that extends southwest towards the coast; and two oriented east-southeast in the northern circumpolar region of Mars. The locations of these six zones are shown in figure 2.

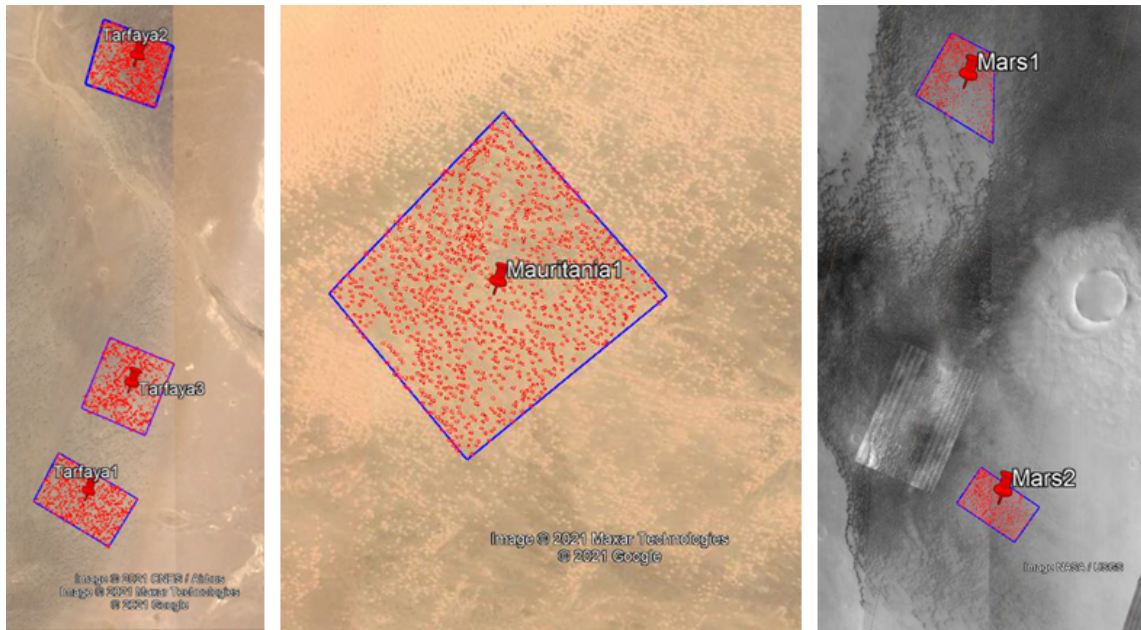


Figure 3: The size zones of study are marked as blue quadrilaterals with the bedforms inside marked in red. The locations of the markers are: Tarfaya1 $22^{\circ}22'10''\text{N}$ $12^{\circ}34'16''\text{W}$, Tarfaya2 $27^{\circ}28'55''\text{N}$ $12^{\circ}33'25''\text{W}$, Tarfaya 3 $27^{\circ}23'50''\text{N}$ $12^{\circ}33'31''\text{W}$, Mauritania1 $19^{\circ}12'20''\text{N}$ $14^{\circ}23'37''\text{W}$, Mars1 $75^{\circ}1'0''\text{N}$ $72^{\circ}8'0''\text{W}$, and Mars2 $73^{\circ}46'0''\text{N}$ $70^{\circ}38'37''\text{W}$. Images courtesy of Google Earth.

Each zone contained at least 1000 bedforms, however not all of the bedforms within the zones were barchan dunes but included also complex dunes, which were likely the intermediate stages of collisions, and bedforms for which no slip-face was visible, these may have been proto-dunes or dome dunes. Aerial images of the six zones are shown in figure 3.

3.2. Measuring dunes

We recorded seven locations on and around each dune body: the toe, the leftmost edge, the tip of the left horn, the base of the slip-face, the brink, the tip of the right horn, and the rightmost edge. These points are shown in figure 4. From these points, it is possible to determine any of the morphological dimensions of the barchan.

Due to the high density of barchans in the zones of study, many of the barchans were not isolated bedforms but were in the process of colliding. In these cases, it was not always possible to identify all seven points on the dunes in which case we attempted to estimate their locations as shown in figure 5. Such an attempt was made in all cases where there were two (or more) distinct crescents in the slip-face. In cases where the leeward slope of a complex bedform exhibited some deformity but only one crescent was visible in the slip-face, the bedform was regarded as a single barchan. In some cases, the bedforms were deformed to such an extent that, although a slip-face was visible, it was no longer crescentic. Such dunes were not recorded as barchans and so no attempt was made to estimate the seven points; instead, we traced around the outline of the dune.

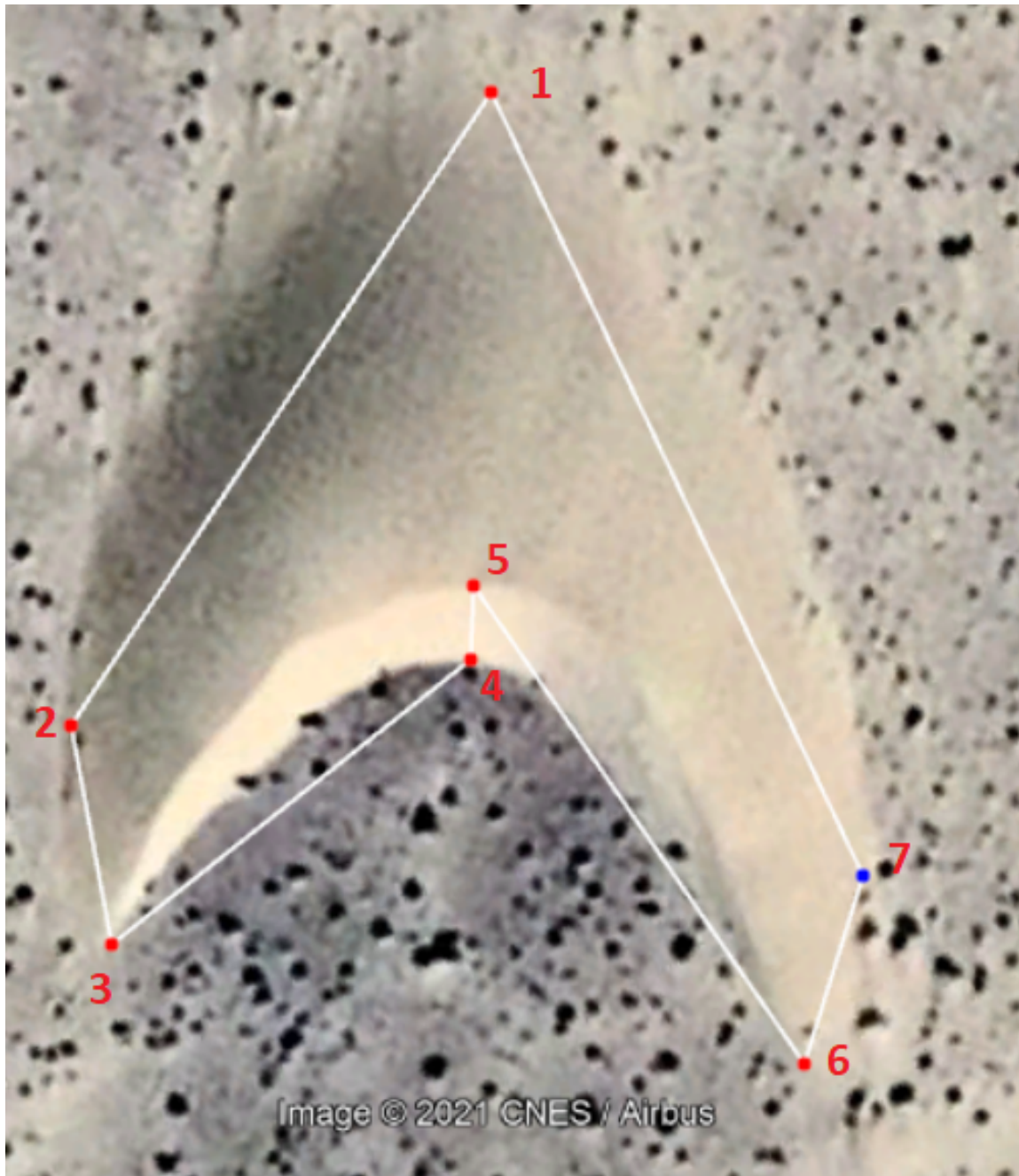


Figure 4: The seven points that were recorded on each barchan within the zones of study. Image courtesy of Google Earth. The dominant wind direction is from the top of the image to the bottom.

In addition to complex bedforms resulting from dune-dune interactions, some bedforms did not have a visible slip-face. When no slip-face was visible, but the shape was otherwise distinctly that of a barchan, it was assumed that the cause was poor image resolution and an attempt was made to estimate the location of all seven points. Where there was no visible slip-face and the shape of the bedform did not appear barchan-like we recorded only four points: the upwind, downwind, leftmost, and rightmost extents of the bedform.

3.3. Determining volumes

From the seven points recorded on each of the barchans, we can calculate any linear dimension of the dunes including horn-to-horn width, total width, windward length, and total length. However, to compare the outputs of the mean-field model to the observations of the real-world fields, it was necessary to calculate the volume of the bedforms from the linear dimensions. Previous studies have shown how the volume of barchans scales as the cubic power of their height, length, and width [4, 35, 36, 16, 12].

We found that the most reliable linear dimension was the length l , the distance between points 1 and 4 shown in figure 4. The length was the easiest dimension to extract since it did not require correction for the orientation of the dune (as was necessary for determining the width). We also found that there was a greater degree of subjectivity in locating exactly the position of the widest point, while sand streaming off of the horns sometimes made defining the tip of the horn difficult. On the other hand, we found that, in most cases, the toe and slip-face were easily identified, making the length measurement more reliable than other dimensions. To calculate the volume v we used the relation $v = l^3/20$ which is a good description of the barchans in the Tarfaya Province [4].

4. Results

We will now describe the observed size distributions, the method by which we optimised model parameters, and the quality of the fits obtained using these optimal configurations. Discussion of the physical relevance of the results will be left for the following section.

4.1. Observed size distributions

As we have mentioned, each of the zones of study contained over 1000 bedforms, however not all of these bedforms were barchan dunes. Since the length-volume relation [4] only holds for barchans, for this work we ignored all other bedforms and worked solely with the barchan size-distributions. The population sizes in Tarafya zones 1, 2, and 3 were 927, 1112, and 850 respectively. The Mauritanian zone contained 984 barchans while Mars 1 and 2 contained 977 and 975 respectively.

4.1.1. Length distributions

In the four terrestrial swarms, the average length of barchans was approximately equal; Tarfaya zones 2 and 3 and the Mauritanian zone all had an average length of 23m while the barchans in Tarfaya 1 were slightly larger with an average of 26m. We observed that the Martian barchans were significantly larger than those on Earth with average lengths of 131m and 113m in Mars zones 1 and 2 respectively. The large discrepancy between dune sizes on Earth and Mars is likely caused by differences in the mechanics of saltation in the two environments [37] but the sizes will also depend

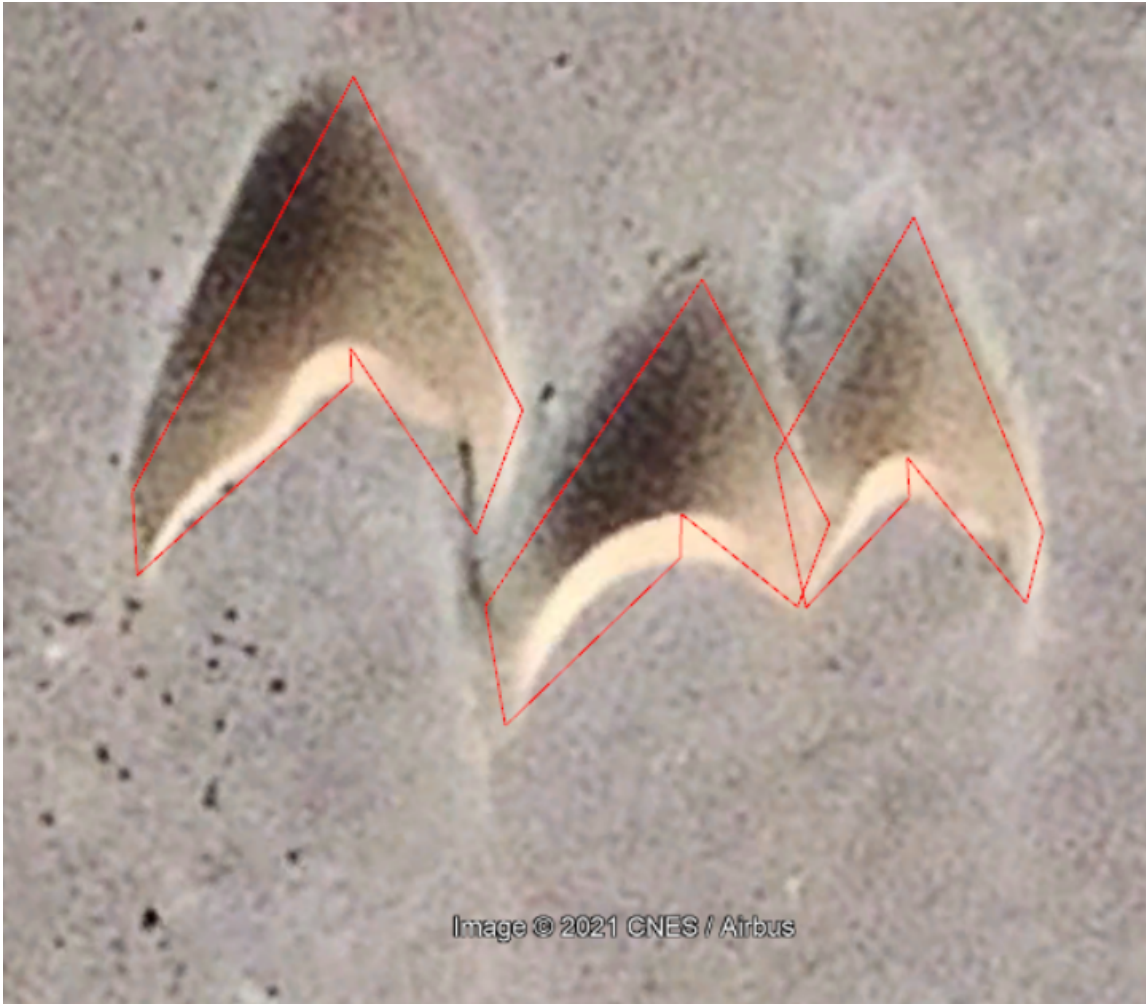


Figure 5: Example of mid-collision barchans where the locations of some of the seven points had to be estimated. Image courtesy of Google Earth

on sediment availability and other factors.

Although understanding these differences is important for understanding dune fields, the average size of dunes in a location is likely controlled by external environmental factors. In this work, we are more interested in understanding how the internal processes of barchan-barchan interactions govern the distribution about this mean. Therefore, for the remainder of this work, we will always normalise lengths (and volumes) by the mean size of barchans in that zone allowing us to compare the results from each of the different areas of study.

Figure 6 shows distributions of normalised length in each of the zones of study. The distributions in the three Tarfaya zones are very similar which is unsurprising since these three zones constitute different areas within a single large population of dunes. The similarity in these three distributions and the similarity in average size in the Tarfaya zones suggests that our assumption of homogeneity in large fields is valid and is in agreement with previous findings [4, 18]. A similar argument could also be made for the two Martian fields, however, it is surprising that the Mauritania zone has a very similar distribution to the fields on Mars despite the large difference in the average size. The striking similarity between the Mauritanian and Martian data suggests that the internal processes in the two locales are similar despite the environmental conditions being very different. These findings also potentially suggest that there may be a certain degree of universality of size distributions, with different classes of barchan fields (e.g. Tarfaya-type, Mars-Mauritania-type).

Although the distributions in the Tarfaya zones are rather different to those in Mauritania and Mars, all of the distributions can be well-approximated by log-normal distributions as has been widely reported in previous studies [4, 17, 18]. This can also be seen in figure 6 where we show log-normal distributions estimated using the method of moments.

4.1.2. Volume distributions

Since we have assumed that the volume of barchan is directly proportional to the cube of its length, a log-normal distribution of lengths would correspond to a log-normal distribution of volumes. However, the slight discrepancies between the observed length and the estimated log-normal distributions are exaggerated when converted to volume distributions. This is particularly obvious in the Tarfaya data, where differences between the distributions close to the peak are particularly emphasised when converted to volumes as shown in figure 7. Note here that it is possible to optimise the parameters of the log-normal distributions to produce a better fit to the data, however, our objective was not to produce arbitrarily accurate empirical fits but rather to investigate how these distributions could be produced solely through the interactions of the dunes.

4.2. Free parameters and optimisation procedure

As described in section 2.3, interactions in the CAFE model are governed by: the distributions of the stochastic variables r_c , r_{f_1} , r_{f_2} , and r_e ; and the rate coefficients α_c , α_a , α_f , and α_e . In all cases, α_a and α_f are not independent and therefore we have only three free rate coefficients. This constraint on a rate coefficient is the only constraint that exists in the CAFE model in general. However, it is not possible to perform a generalised optimisation of the model since infinitely many free parameters would be required to describe all of the possible distributions for the stochastic variables. To perform the optimisation, we, therefore, restrict ourselves to three specific implementations of the CAFE model:

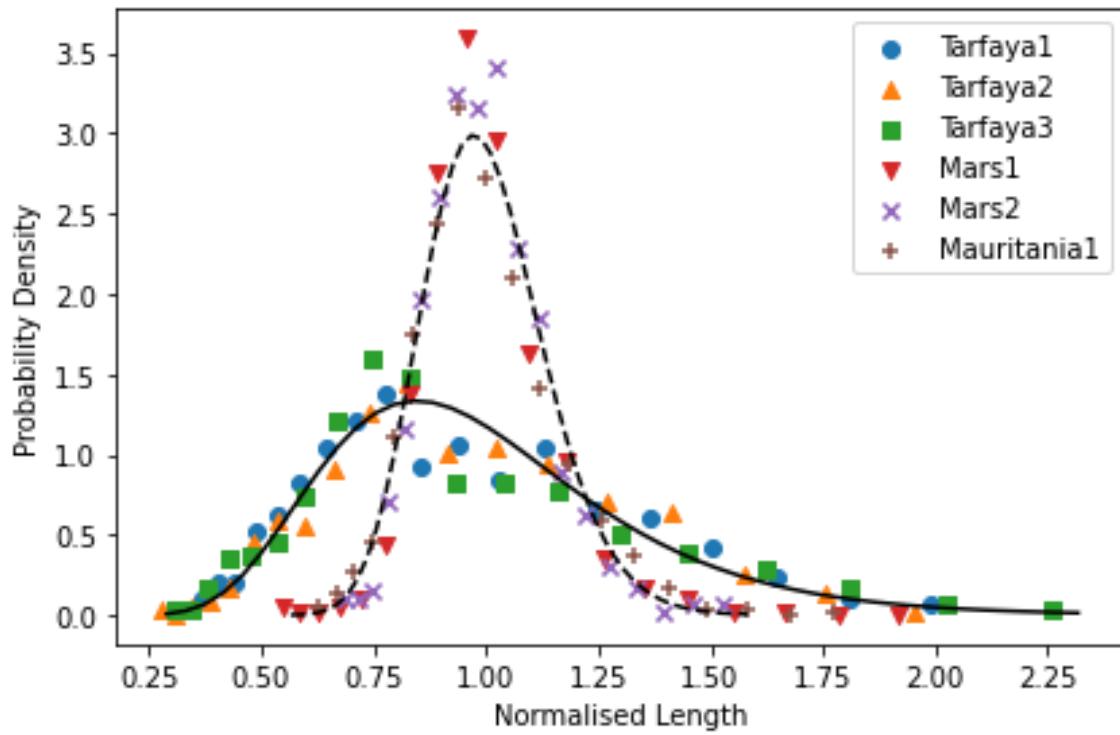


Figure 6: Probability density functions are shown for the lengths of barchans in each of the six zones of study normalised by the average length in that zone. The lines show log-normal distributions estimated from the mean and variance of the observed data.

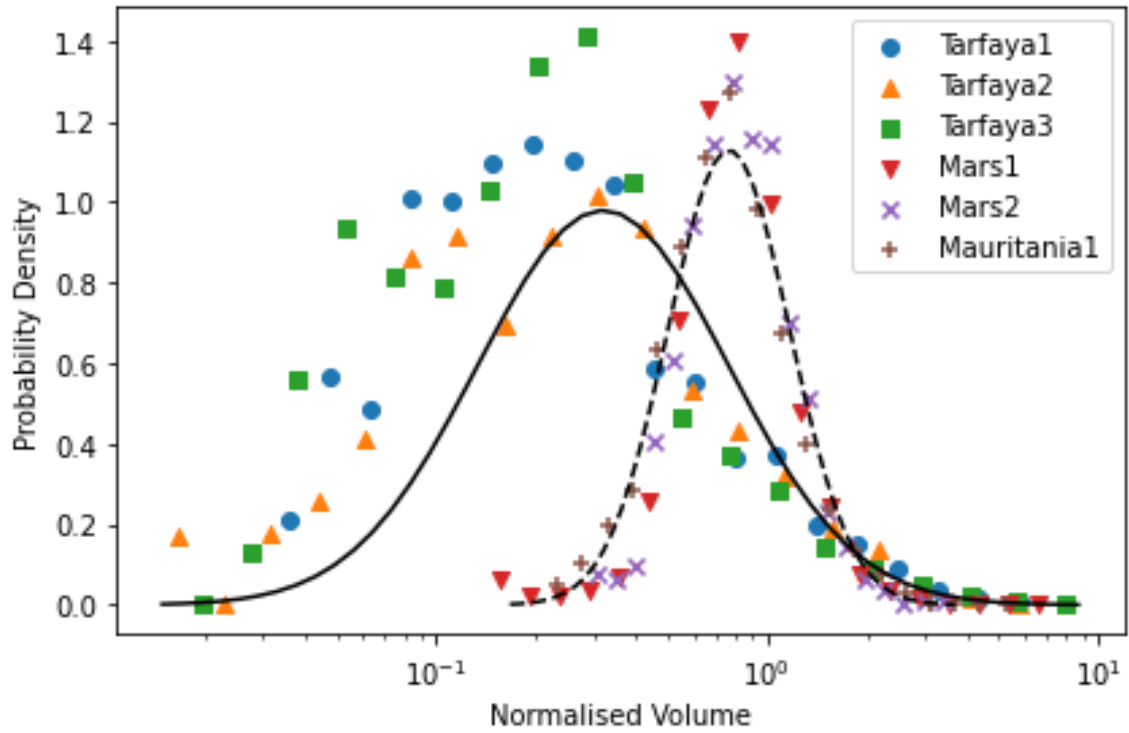


Figure 7: Observed probability density functions of barchan volumes calculated as $v = l^3/20$ in the zones of study. The lines show log-normal distributions estimated from the moments of the combined distributions of all three Tarfaya zones (solid line) and the Martian and Mauritanian zones (dashed line).

Model	α_c	α_a	α_f	α_e
AFE	$\alpha_c = 0$	$\alpha_a = (1 - \alpha_e)/2$	$\alpha_f = (1 - \alpha_e)/2$	Free
CAE	Free	$\alpha_a = 2\alpha_c/(N - 1)$	$\alpha_f = 0$	Free
CAFE	Free	$\alpha_a = 2\alpha_c/(N - 1) + \alpha_f$	Free	Free

Table 1: The rate coefficients in the uniform AFE, uniform CAE, and empirical CAFE models. Where an equality is shown the parameter is constrained to take that value.

- The uniform AFE model where: $\alpha_c = 0$, $\alpha_a = \alpha_f = (1 - \alpha_e)/2$, and the stochastic variables r_{f_1} , r_{f_2} , and r_e are each distributed uniformly in the ranges $[r_{f_1_{min}}, r_{f_1_{max}}]$, $[r_{f_2_{min}}, r_{f_2_{max}}]$, and $[r_{e_{min}}, r_{e_{max}}]$ respectively.
- The uniform CAE model where: $\alpha_c \neq 0$, $\alpha_f = 0$, and $\alpha_a = 2\alpha_c/(N - 1)$. The stochastic variables r_c and r_e are distributed uniformly in the ranges $[r_{c_{min}}, r_{c_{max}}]$ and $[r_{e_{min}}, r_{e_{max}}]$ respectively.
- The empirical CAFE model where: $\alpha_c \neq 0$, $\alpha_a = 2\alpha_c/(N - 1) + \alpha_f$, the distributions of r_{f_1} and r_e are determined from a known collision rule, and the distributions of r_c and r_{f_2} are uniformly distributed in $[r_{c_{min}}, r_{c_{max}}]$ and $[r_{f_2_{min}}, r_{f_2_{max}}]$ respectively.

The uniform AFE and empirical CAFE model have 7 free parameters while the CAE model has 6. These are shown, together with the constraints in tables 1 and 2.

The dimensionality of the parameter spaces in these three model versions is low enough that the optimisation algorithm (described in section 4.2.2) converged, for different initial conditions, in a reasonable amount of time to a single minimum in each zone. Despite the reduction in parameters, our choice of these three implementations allows for a wide investigation of the power of the general CAFE model. The uniform AFE and CAE models sacrifice one of the types of interaction but allow us to maintain the adjustability of the rules for the remaining processes. Comparison of these two models allows us to comment upon how changing from calving to collisional fragmentation affects the size distribution. Note also that we use uniform distributions for the stochastic variables as, in this case, each of the terms appearing in equation (18) has an exact form.

The empirical CAFE model sacrifices some of the adjustability of the other models but includes all of the processes. The distributions of r_e and r_{f_1} are derived from a rule thought to be applicable to real-world barchan collisions [17, 12, 18] and therefore the empirical CAFE model ought to be realistic. However, none of the model implementations includes long-range interactions of barchans in a swarm via exchange of sand flux. This means that the empirical CAFE model may not be able to accurately reproduce distribution in swarms where sand flux plays a dominant role. On the other hand, in the uniform AFE and CAE, the interaction rules can adjust themselves to compensate for the lack of sand flux, and therefore may be able to give a better fit.

4.2.1. Empirical collision rule

In the empirical CAFE model we fix the distributions $p_{f_1}(r_{f_1})$ and $p_e(r_e)$ to a distribution we derived using an empirical collision rule [17, 18]. The collision rule was developed by empirically fitting the volume ratio of outputs of barchan-barchan collisions to a function of their lateral offset and initial volume ratio [17, 12]. The details of the rule can be found in the appendix of [18]. The

Model	$p_c(r_c)$	$p_{f_1}(r_{f_1})$	$p_{f_2}(r_{f_2})$	$p_e(r_e)$
AFE	n/a	$[r_{f_1_{min}}, r_{f_1_{max}}]$	$[r_{f_2_{min}}, r_{f_2_{max}}]$	$[r_{e_{min}}, r_{e_{max}}]$
CAE	$[r_{c_{min}}, r_{c_{max}}]$	n/a	n/a	$[r_{e_{min}}, r_{e_{max}}]$
CAFE	$[r_{c_{min}}, r_{c_{max}}]$	Empirical	$[r_{f_2_{min}}, r_{f_2_{max}}]$	Empirical

Table 2: The distributions of the four stochastic variables in the uniform AFE, uniform CAE, and empirical CAFE models. We have used the shorthand $[x, y]$ to denote a uniform distribution in the range $[x, y]$. In all such cases, x and y are free model parameters. The empirical distributions were derived from a known collision rule.

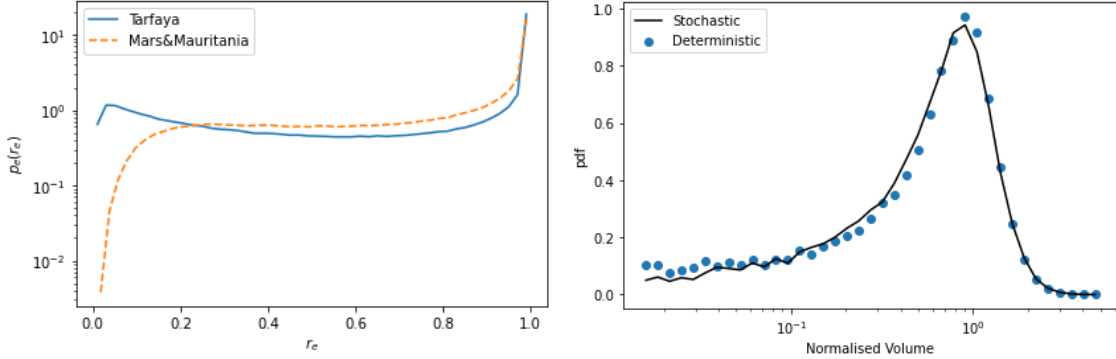


Figure 8: Left: The distributions used for r_e and r_{f_1} in the empirical CAFE model for Tarfaya datasets (solid line) and the Mars and Mauritania datasets (dashed line). Right: A comparison of the steady-state distribution produced using the deterministic collision rule [18] and the stochastic collision rule we derived from the deterministic one.

collision rule has previously been used in mean-field modelling for exchange collisions only [17], however, we also took the ratio r_{f_1} to be given by the same rule since many fragmentation collisions are similar to an exchange collision where one of the outputs subsequently breaks apart.

The empirical collision rule is deterministic given the initial volume ratio and lateral offset [18]. To implement this rule in the CAFE model we had to convert the deterministic expression into a probability distribution of outputs. The method for doing this was:

1. Randomly select two dunes from our steady-state population and calculate their volume ratio r_{in} .
2. Generate a random value for the lateral offset θ from a uniform distribution in the range $[0, 1]$.
3. Insert r_{in} and θ into the deterministic collision rule [18] to give the output volume ratio r_{out} .
4. Record r_{out} and repeat until 10^6 values have been generated.

When running the empirical CAFE model, each time we were required to generate a random value for r_e or r_{f_1} we simply randomly selected one of these 10^6 deterministically calculated r_{outs} . The resulting distributions for our datasets are shown in the left part of figure 8.

Before we proceeded with implementing this method using our real-world data, we first ensured that the outputs generated from our stochastic distribution were the same as those generated when using the deterministic rule itself. An example of this is shown in the right part of figure 8

4.2.2. Optimisation

Since we can solve for the steady-state distribution for a particular configuration of the CAFE model, one method of optimising the parameters would have been to use some measure of similarity between distributions, such as the Kolmogorov-Smirnov (KS) test statistic. as a cost function of an optimisation routine. However, the time taken to solve for the steady-state, and the high dimensionality of the parameter space, mean we would only be able to explore a small area of the space using this technique. Instead, we chose to make use of the fact that we have analytical expressions for all of the integer moments (equation (17)). The computational time taken to solve for the moments of the steady-state is therefore much less than solving for the entire steady-state. We, therefore, defined a cost function as the average percentage difference between the first 9 non-trivial moments of the observed and theoretical normalised volume distributions (since the volumes are normalised, the first moment is unity) i.e.

$$\lambda = \frac{1}{9} \sum_{\ell=2}^{10} \sqrt{\frac{(\mathbf{E}[v^\ell] - \langle v^\ell \rangle_s)^2}{\mathbf{E}[v^\ell]^2}}, \quad (20)$$

where $\mathbf{E}[v^\ell]$ are the observed moments and $\langle v^\ell \rangle_s$ are the theoretical steady-state moments for a given set of parameters calculated using equation (17). This cost function minimises the average percentage error of the moments which, since the moments are rapidly increasing, means that the cost function prefers models where the lower moments are close to the data and puts less constraint on the higher moments. This is important since the lower moments are more stable to the presence of large outliers. We also found that implementing the generalised method of moments using weightings calculated from a heteroskedasticity-consistent covariance matrix did not converge to an optimum configuration within the permitted range of parameters (e.g. $r_{e_{min}} \in [0, 1]$ etc.)

The optimisation of the model then consisted of finding the global minimum of our cost function. We performed this minimisation using the SciPy [38] implementation of dual annealing, a technique which couples generalised annealing with a local search [39, 40, 41, 42, 43].

The generalised annealing searched through $\sim 3 \times 10^5$ configurations of the parameters. When the local search was included this increased to $\sim 10^6$ parameter configurations. We ran the optimisation algorithm for each of the three models and for:

- Each of the three Tarfaya zones separately.
- The combined distribution of all three Tarfaya zones.
- Both of the Mars zones and the Mauritania zone separately.
- The combined distribution of both Mars zones and the Mauritania zone.

Altogether this meant that 24 runs of the dual annealing were performed, in all of which the algorithm converged to a minimum. We chose to group distributions in the way described above to give larger data sets. We feel that this is also reasonable since the distributions appeared very similar as shown in figures 6 and 7, suggesting the internal interactions were very similar.

4.3. Optimum parameters

We ran the population dynamics algorithm to find the steady-state distribution corresponding to the optimum parameters we had found. We found that a small number of very large outliers in Mars zone 1 and the Mauritania zone were significantly changing the observed moments in those fields which led to the optimum parameters producing steady-states which were significantly different to the observed distributions. Removing these outliers (five in Mars zone 1 and two in the Mauritania zone) resulted in the optimum parameters producing steady-state distributions that were much closer to the observation.

We show optimum parameters configurations for all of the observed distributions in table 3 for the uniform AFE, uniform CAE, and empirical CAFE models respectively. To help with comparison between the rate coefficients for calving and the collision process, we define *event probabilities* ρ_i with $i = c, a, f, \text{ or } e$

$$\rho_c = \frac{\alpha_c N}{\alpha_c N + (\alpha_a + \alpha_f + \alpha_e)N(N-1)/2}, \quad (21)$$

$$\rho_{a,f,e} = \frac{\alpha_{a,f,e}N(N-1)}{2\alpha_c N + (\alpha_a + \alpha_f + \alpha_e)N(N-1)}. \quad (22)$$

These event probabilities, $\rho_{c,a,f,e}$, are the probabilities the next event (calving or collision) to occur in the system will be calving, aggregation, fragmentation, or exchange accounting for the different dependence of the rate coefficients on population size. Note also that since these four events are the only processes in our model $\rho_c + \rho_a + \rho_f + \rho_e = 1$. In the case of the uniform AFE model $\rho_a = \rho_f = (1 - \rho_e)/2$ since the rates of fragmentation and aggregation must balance in order for a steady-state to exist. Similarly, in the uniform CAE model $\rho_a = \rho_c$ and in the empirical CAFE model $\rho_a = \rho_c + \rho_f$.

Across the three different models, we observe certain similarities in the optimised parameters. First and foremost we see that $\rho_e > 0.50$ in all cases and $\rho_e > 0.8$ in most instances. This means that exchange collisions make up the majority of interactions regardless of the model chosen which is in agreement with simulations of barchan-barchan collisions where exchange interactions are observed to result from the greatest range of input parameters [17].

Fragmentation and aggregation were found to be uncommon when using the uniform AFE with the most frequent occurrence found for the combined Tarfaya dataset where $\rho_a = \rho_f = 5.5\%$. Likewise, in the uniform CAE model the relative probabilities of calving and aggregation collisions were $\rho_c = \rho_a < 2.5\%$. The highest optimised rates of non-exchange interactions were found using the empirical CAFE model which found probabilities $\rho_a \approx \rho_f = 0.23$ for Tarfaya 3. The optimised empirical CAFE parameters for Mars 1 were $\rho_c \approx \rho_a = 9.2\%$ which was the highest value for the probability of calving observed in any of the fields.

In the Tarfaya zones, the uniform AFE and uniform CAE converged to the same result, where exchange collisions were considerably more frequent than the other types of interactions, and the average volume ratio of the outputs of an exchange collision was in the range $[0.2, 0.3]$ (i.e. on average one output was between 3.3 and 5 times larger than the other). It is also worth noting

that the optimum model parameters relating to the distributions of r_{f_1} and r_{f_2} (in the uniform AFE model) were found to be very similar in all of the zones with $r_{f_{1min}} = 1.0$, $r_{f_{1max}} = 2.8$, and $r_{f_{2min}} = r_{f_{2max}} = 1.0$ found to be the optimum in all but one case. These distributions of r_{f_1} and r_{f_2} mean that the outputs of fragmentation collision are two equally sized small dunes and then a larger dune with a volume between 2 and 5.6 times as large as each of the small dunes. Fragmentation of this type, where the result is one large dune and two similarly sized smaller dunes, has been seen in both water tanks experiments and simulations of barchan collisions (e.g. centred “fragmentation-chasing” in [21] and “budding” in [44]). In contrast, for the empirical CAFE model, r_{f_2} was found to only take very small values, i.e. one of the two smaller dunes is much larger than the other, this is more similar to the “neighbouring effect” described in [19].

The calving parameters were found to be less consistent for the different zones than the fragmentation rules. In the uniform CAE the size of the smaller dune was always in the range 44-100% of the size of the larger output of calving however the exact values varied significantly between the zones. This type of calving is very different to how the process is understood in the real world, where r_c ought to be a lot smaller since only large dunes calve and the new dune is created at the minimum size [28, 19]. The rule for calving in the empirical CAFE model is much more in line with that conception of the process.

Finally, it may seem surprising at first that the optimal parameters for the combined distribution of several zones may differ significantly from those found for the zones individually. For instance, one can see in table 3 that $\rho_e = 1.0$ in each of the Tarfaya zones individually however, when combined, the optimum value obtained was $\rho_e = 0.89$. This can be explained by looking at the optimum parameters of the stochastic variables in these instances. We can see that in each of the individual zones $r_{e_{min}} \approx r_{e_{max}}$ in which case (bearing in mind $\rho_e = 1.0$ for the individual zones) the theoretical moments are

$$\langle v^\ell \rangle_i = \frac{1 + r_i^\ell}{(1 + r_i)^\ell}, \quad (23)$$

where we use $i = 1, 2, 3$ to represent Tarfaya 1, 2, and 3 respectively and $r_i = r_{e_{min}}^{(i)} = r_{e_{max}}^{(i)}$. The combined distribution has moments

$$\langle v^\ell \rangle_{tot} = \sum_{i=1}^3 \frac{N_i \langle V^\ell \rangle_i}{N_{tot}}, \quad (24)$$

where N_i is the population size of that zone and $N_{tot} = N_1 + N_2 + N_3$ is the total population size of all three zones. Owing to the non-linearity of equation (23), the total moments cannot generally be re-written in the same form i.e. there does not, in general, exist an r for which

$$\langle v^\ell \rangle_{tot} = \frac{1 + r^\ell}{(1 + r)^\ell}. \quad (25)$$

Hence, the optimum parameter configuration for the combined dataset does not look the same as any of the individual zones. Similar arguments can be applied to the other discrepancies between the combined datasets and their constituents in the other models.

Model&Zone	ρ_c	ρ_a	ρ_f	ρ_e	$r_{C_{min}}$	$r_{C_{max}}$	$r_{f_{min}}$	$r_{f_{max}}$	$r_{f_{min}}$	$r_{f_{max}}$	$r_{e_{min}}$	$r_{e_{max}}$
AFE T1	n/a	neg.	neg.	1.0	n/a	n/a	n/c	n/c	n/c	n/c	0.27	0.27
AFE T2	n/a	neg.	neg.	1.0	n/a	n/a	n/c	n/c	n/c	n/c	0.29	0.29
AFE T3	n/a	neg.	neg.	1.0	n/a	n/a	n/c	n/c	n/c	n/c	0.20	0.20
AFE TALL	n/a	0.054	0.054	0.89	n/a	n/a	1.0	2.8	1.0	1.0	0.23	0.25
AFE M1	n/a	0.014	0.014	0.97	n/a	n/a	1.0	2.8	1.0	1.0	0.27	0.98
AFE M2	n/a	0.043	0.043	0.91	n/a	n/a	1.0	2.8	1.0	1.0	0.31	1.0
AFE Mau.	n/a	0.016	0.016	0.97	n/a	n/a	1.0	2.8	1.0	1.0	0.21	1.0
AFE MMau.	n/a	0.027	0.027	0.95	n/a	n/a	0.98	4.22	0.89	1.0	0.26	0.99
CAE T1	neg.	neg.	n/a	1.0	n/c	n/c	n/a	n/a	n/a	n/a	0.27	0.27
CAE T2	neg.	neg.	n/a	1.0	n/c	n/c	n/a	n/a	n/a	n/a	0.29	0.29
CAE T3	neg.	neg.	n/a	1.0	n/c	n/c	n/a	n/a	n/a	n/a	0.20	0.20
CAE TALL	0.012	0.012	n/a	0.98	0.82	0.86	n/a	n/a	n/a	n/a	0.10	0.40
CAE M1	2.2×10^{-3}	2.2×10^{-3}	n/a	1.0	1.0	1.0	n/a	n/a	n/a	n/a	0.23	1.0
CAE M2	0.023	0.023	n/a	0.95	0.57	0.69	n/a	n/a	n/a	n/a	0.25	1.0
CAE Mau.	3.8×10^{-3}	3.8×10^{-3}	n/a	0.99	0.70	0.93	n/a	n/a	n/a	n/a	0.18	1.0
CAE MMau.	0.013	0.013	n/a	0.97	0.67	0.75	n/a	n/a	n/a	n/a	0.22	1.0
CAFE T1	2.8×10^{-3}	0.10	0.10	0.79	0.047	0.075	n/a	n/a	8.9×10^{-4}	2.9×10^{-3}	n/a	n/a
CAFE T2	2.1×10^{-3}	0.082	0.080	0.84	4.6×10^{-3}	0.19	n/a	n/a	7.1×10^{-4}	1.9×10^{-3}	n/a	n/a
CAFE T3	9.1×10^{-4}	0.23	0.23	0.53	0.083	0.11	n/a	n/a	1.1×10^{-3}	1.5×10^{-3}	n/a	n/a
CAFE TALL	neg.	0.18	0.18	0.63	0.21	0.25	n/a	n/a	3.3×10^{-6}	6.3×10^{-6}	n/a	n/a
CAFE M1	0.091	0.092	7.3×10^{-4}	0.82	0.93	0.94	n/a	n/a	0.11	0.66	n/a	n/a
CAFE M2	neg.	neg.	neg.	1.0	n/c	n/c	n/a	n/a	n/c	n/c	n/a	n/a
CAFE Mau.	9.6×10^{-3}	9.6×10^{-3}	neg.	0.98	0.94	0.99	n/a	n/a	n/c	n/c	n/a	n/a
CAFE MMau.	neg.	neg.	neg.	1.0	n/c	n/c	n/a	n/a	n/c	n/c	n/a	n/a

Table 3: The optimum parameters for the uniform AFE, uniform CAFE, and empirical CAFE models for all datasets which were: the three Tarfaya zones (T1, T2, T3), the combined Tarfaya dataset (TALL), the two Martian zones (M1, M2), the Mauritania zone (Mau.), and the combined Mars+Mauritania dataset (MMau.). Event probabilities $\rho_{c,a,f,e}$ marked “neg.” had optimum values smaller than $\mathbf{O}(10^{-5})$ or smaller. Values marked “n/a” were not applicable to that model while entries marked “n/c” were not constrained since the relevant event probability was negligible.

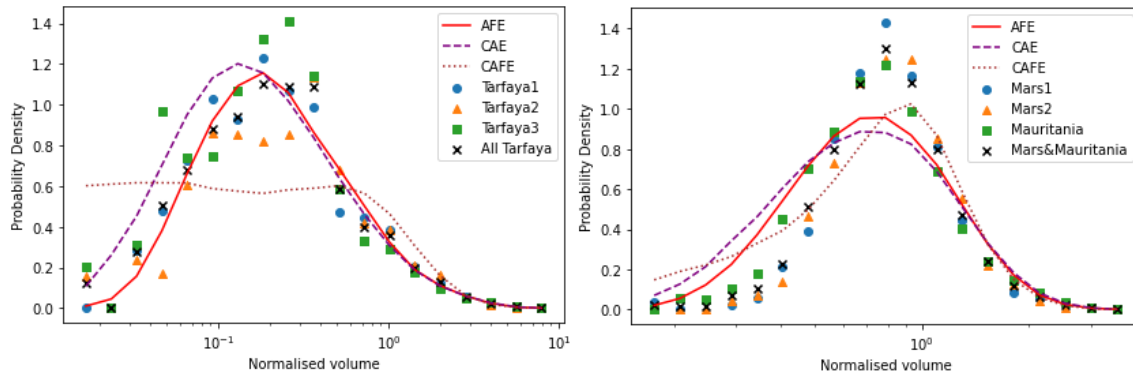


Figure 9: The normalised steady-state volume distributions corresponding to the optimised parameters for the uniform AFE, uniform CAE, and empirical CAFE models for: the combined distribution of all three Tarfaya zones (left) and the combined distributions of the two Martian zones and the Mauritanian zone (right) with the data from the fields themselves shown as points.

4.4. Steady-state distributions

The parameters were inserted into a population dynamics algorithm [27, 32, 33] to find their corresponding steady-state distributions. In figure 9 we show the volume distributions of steady-states for the optimised parameters calculated for: the combined distribution of the three Tarfaya zones and the combined distribution of the Martian and Mauritanian zones. One can see that reasonable fits are achieved in both cases for the uniform AFE and uniform CAE models while the empirical CAFE model gives a very poor fit to the Tarfaya data. Since the raw data we obtained was the lengths of the dunes we also show the steady-state length distributions in figure 10

To quantitatively evaluate the strength of each fit we calculated two-sample KS statistics from the raw datasets and the steady-state outputs of the three models. The KS statistics for the three models and a log-normal estimated from the first two moments are shown in table 4. From these KS statistics, we can see that the uniform AFE and uniform CAE can produce steady-state distributions which fit the data more accurately than a log-normal in the case of the Tarfaya datasets while the empirical collision rule CAFE model yields a much poorer fit (though still comparable to the log-normal). In the case of the Martian and Mauritanian data, we see that the uniform AFE and empirical CAFE generally give similar fits to the data while the uniform CAE model gives a worse fit. For the Martian and Mauritanian data, the estimated log-normal gives a better fit than any of the models.

5. Discussion of results

The fact that the Martian and Mauritanian datasets appear to fit one another very closely is surprising. Given the large differences between the environments of Mars and Mauritania their close fit strongly suggests that it is indeed the internal processes of dune interactions that govern the shape of the size distributions, with external controls determining the average size.

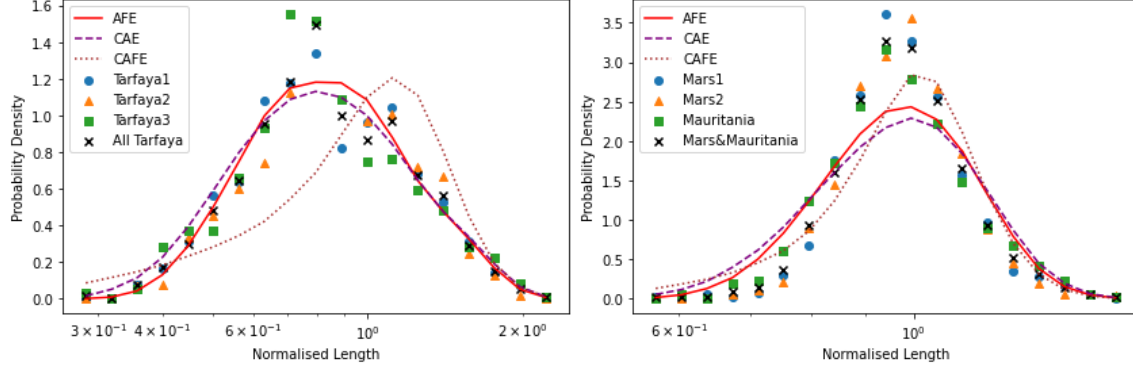


Figure 10: The steady-state distributions of normalised length corresponding to the optimised parameters for the uniform AFE, uniform CAE, and empirical CAFE models for: the combined distribution of all three Tarfaya zones (left) and the combined distributions of the two Martian zones and the Mauritanian zone (right), with the data from the fields themselves shown as points.

	AFE	CAE	CAFE	log-normal
Tarfaya1	0.051	0.050	0.13	0.11
Tarfaya2	0.033	0.033	0.13	0.10
Tarfaya3	0.073	0.077	0.15	0.11
Tarfaya1&2	0.037	0.041	0.12	0.11
All Tarfaya	0.026	0.044	0.12	0.10
Mars1	0.086	0.10	0.16	0.084
Mars2	0.077	0.11	0.079	0.036
Both Mars	0.083	0.11	0.078	0.038
Mauritania	0.072	0.089	0.076	0.041
Mars and Mauritania	0.078	0.10	0.063	0.037

Table 4: Two-sample Kolmogorov-Smirnov (KS) statistics calculated between the observed distributions and the optimised model steady-states for the three models and all of the different datasets. For reference we have also included KS statistics for log-normal distributions with parameters estimated from the first two moments.

Our choice to fit combined datasets as well as individual zones led to the important finding that the optimum interaction rules for combined distributions could be very different to those in each of their constituent parts. Although this seems counterintuitive, we have already argued why this is the case in the AFE model, and similar arguments can be applied in the other models. This finding suggests that the most important role played by calving, fragmentation, and aggregation is to generate slight variations between the local distributions in different parts of a swarm. Qualitatively the distributions in the three Tarfaya zones seem to be roughly the same and so homogeneity appears to hold fairly well for the swarm as a whole. However, the subtle differences between these zones mean that the global distribution cannot be accurately reproduced without the inclusion of non-exchange processes. Swarms in which calving, aggregation, or fragmentation are prevalent are likely, therefore, to exhibit greater zonal differences in size distribution.

Comparing the fits (table 4) of the uniform AFE and uniform CAE models to the data, we see that, except in the cases where the two had converged to the same result, the AFE model gives a better fit to the data than does the CAE model. This result implies that fragmentation, especially where the two smaller outputs are similarly sized, is more likely than calving to play the role of driving regional variations as described above. However, in the empirical CAFE model, fragmentation collisions are preferred for the Tarfaya datasets while calving is preferred for the Mars and Mauritania data. Our results are therefore inconclusive as to whether calving or fragmentation is more important in barchan swarms although, in either case, exchange collisions are the dominant interaction.

In the case of the Martian and Mauritanian data, we saw that the fits produced by the empirical CAFE model were much better than in the case of the Tarfaya dunes. An important process in the development of barchan swarms that we have omitted is that of sand flux between the dunes. In previous mean-field modelling where the deterministic collision rule that we adapted was used, the distributions produced using only exchange collisions were then deformed in such a way as to try and mimic the role of sand flux [17]. In that work, the amount of deformation required to match the collision-only steady-state distribution to the real-world distributions was used to infer how relevant sand flux was compared to collisions in each field [17]. Using the same logic, we might therefore conclude that, assuming the empirical collision rule is applicable in Mauritania and on Mars, sand flux plays much less of a role in those settings than in Tarfaya. However, in a later work using the same deterministic collision rule as in [17] it was found that exchange collisions alone could not negate the coarsening effect whereby average dune size increases with downwind distance due to sand flux [18]. The authors of that work concluded that fragmentation processes must therefore be involved to counteract this, however, we found that the optimum rates of calving (spontaneous fragmentation) and collisional fragmentation were small in the Martian and Mauritanian fields (see ρ_c and ρ_f in table 3) and therefore it is unlikely that they would be able to undermine this coarsening effect. It, therefore, remains an open question as to how homogeneity might arise in barchan fields despite sand flux, given that both the simulations of collisions [17] and our work suggest that the overall rate of fragmentation is low. A possible explanation of this is that large barchans undergo calving at a much greater rate than smaller ones, or that there is some minimum size for calving to occur [28, 20], which was not considered in our model.

Another point that can be made from our model is that, especially in the case of the Martian and Mauritanian dunes, the differences between the distribution produced using our three model

implementations are not very significant (see figure 10). Considering this, and the fact that other authors have been able to produce similar distributions using different modelling [17], we can see that it is likely that the size distribution of barchans alone is not enough to determine the nature of interactions in swarms. This suggests one must consider other properties of the fields such as the spatial structuring.

It is worth noting also that our results indicate that a log-normal is not necessarily an entirely accurate description of the distribution of barchan sizes. In figure 6 we show log-normals that quite closely replicate the observed length distributions. However, when we convert the lengths to volumes, the differences between the log-normal and actual distributions are more pronounced and it becomes less obvious that the log-normal distribution is an accurate description, especially in the case of the Tarfaya data. Indeed, we are able to produce distributions using the uniform AFE and uniform CAE models that provide a much closer fit to the Tarfaya distributions than does a log-normal. The reported log-normal fit for a length (or other linear dimensions) distribution may therefore be, in part, due to the volume-length (or volume-width) scaling laws for barchans.

Finally, we have shown that it is possible to produce good fits to the size distributions we observed for barchan swarms in nature using three different implementations of the CAFE model. In previous modelling, [17] many characteristics of these distributions have also been reproduced in models where interactions are treated very differently. This implies that there is not enough information contained in global size distributions in barchan swarms to precisely constrain the interaction rules. For this reason, while it is theoretically possible to extend the CAFE model to include sand flux and a different treatment of calving, we do not feel that these additional factors would lead to greater insight. However, the fact that our finding that exchange collisions are dominant agrees with continuum simulations [17, 12] suggests that, although global size distributions are not sufficient to precisely determine the interaction rules, there is enough information to provide some constraint. This type of modelling remains very useful, therefore, in understanding the role of interactions in shaping barchan size distributions. Rather than proceeding to add to the complexity of a mean-field model, extensions to this work should focus on adding additional information in the form of spatial structuring in barchan swarms and extending the model to be spatially explicit e.g. an agent-based model rather than a mean-field one.

6. Conclusion

We applied a mean-field particle-collision model representing calving, aggregation, fragmentation, and exchange (CAFE) interactions between migrating dunes in barchan swarms to replicate their measured size distributions on Mars and Earth, with three sample areas near Tarfaya, Morocco, one in Mauritania, and two in the Mars' northern circumpolar region.

Fitted model parameters reveal the relative importance of the interaction types and the potential role played by sand flux.

Two distinct classes of distributions were observed: 1) Mars and Mauritania exhibit strikingly similar size distributions, suggesting that the interactions are comparable despite the different planetary environments; 2) the three Tarfaya sample areas show similar size distributions and model results imply that sand flux is more important in these swarms. The optimised model steady-state

solutions give reasonable fits to the size distributions in the swarms, in several cases providing a better fit than the expected log-normal distribution. The results show that exchange is the dominant interaction type for all swarms making up at least 53%, and more typically $> 80\%$, of events. Fragmentation and aggregation are much less prevalent, making up at most 23% of events each, and more often $< 10\%$. Calving is found to represent $\lesssim 1\%$ of events in most instances, with the highest rate found to be 9.1%. Generally, the fits produced by the models are better when the rate of non-exchange interactions is low. The results suggest that collisions, especially exchange, play a more important role than calving in shaping size distributions in barchan swarms. We furthermore find that processes other than exchange are most important in swarms where there are local variations in the size distribution.

Including sand flux and adapting calving so that only larger barchans are able to calve are possible extensions to the model. However, both would prevent the analytical calculation of the moments. Additionally, we have been able to replicate the distributions using different implementations of a model and other authors have also been able to reproduce similar distributions using other types of models. This suggests that there is not enough information contained within the global size distribution alone. Nevertheless, the results we have presented provide some answers to open questions on the roles of calving, collision, and sand flux in barchan swarms.

Acknowledgments

DTR is supported by the EPSRC Centre for Doctoral Training in Cross-Disciplinary Approaches to Non-Equilibrium Systems (CANES EP/L015854/1).

References

- [1] Mary C Bourke and Andrew S Goudie. Varieties of barchan form in the namib desert and on mars. *Aeolian Research*, 1(1-2):45–54, 2009.
- [2] Andrew S Goudie. Global barchans: A distributional analysis. *Aeolian Research*, 44:100591, 2020.
- [3] Ralph A Bagnold. *The Physics of Blown Sand and Desert Dunes*. Methuen, London, 1941.
- [4] Hicham Elbelrhiti, Bruno Andreotti, and Philippe Claudin. Barchan dune corridors: field characterization and investigation of control parameters. *Journal of Geophysical Research: Earth Surface*, 113(F2), 2008.
- [5] S Parker Gay Jr. Observations regarding the movement of barchan sand dunes in the nazca to tanaca area of southern peru. *Geomorphology*, 27(3-4):279–293, 1999.
- [6] El-Sayed Sedek Abu Seif and Mohamed H El-Khashab. Desertification risk assessment of sand dunes in middle egypt: a geotechnical environmental study. *Arabian Journal for Science and Engineering*, 44(1):357–375, 2019.
- [7] MA Hamdan, AA Refaat, and M Abdel Wahed. Morphologic characteristics and migration rate assessment of barchan dunes in the southeastern western desert of egypt. *Geomorphology*, 257:57–74, 2016.
- [8] Ammar Amin and El-Sayed Sedek Abu Seif. Environmental hazards of sand dunes, south jeddah, saudi arabia: an assessment and mitigation geotechnical study. *Earth Systems and Environment*, 3(2):173–188, 2019.
- [9] Bin Yang, Yong Su, Nan He, Bo Zhang, Xiaosi Zhou, and Yang Zhang. Experimental study on the stable morphology and self-attraction effect of subaqueous barchan dunes. *Advanced Powder Technology*, 31(3):1032–1039, 2020.
- [10] Junhuai Yang, Zhibao Dong, Zhengyao Liu, Weikang Shi, Guoxiang Chen, Tianjie Shao, and Hanmin Zeng. Migration of barchan dunes in the western quruq desert, northwestern china. *Earth Surface Processes and Landforms*, 44(10):2016–2029, 2019.
- [11] Fangen Hu, Xiaoping Yang, and Hongwei Li. Origin and morphology of barchan and linear clay dunes in the shuhongtu basin, alashan plateau, china. *Geomorphology*, 339:114–126, 2019.
- [12] Orencio Durán, Eric JR Parteli, and Hans J Herrmann. A continuous model for sand dunes: Review, new developments and application to barchan dunes and barchan dune fields. *Earth Surface Processes and Landforms*, 35(13):1591–1600, 2010.
- [13] Bruno Andreotti, Philippe Claudin, and S Douady. Selection of dune shapes and velocities part 2: A two-dimensional modelling. *The European Physical Journal B-Condensed Matter and Complex Systems*, 28(3):341–352, 2002.
- [14] Pascal Hersen, Ken Haste Andersen, Hicham Elbelrhiti, Bruno Andreotti, Philippe Claudin, and Stéphane Douady. Corridors of barchan dunes: Stability and size selection. *Physical Review E*, 69(1):011304, 2004.

- [15] Klaus Kroy, Gerd Sauer mann, and Hans J Herrmann. Minimal model for aeolian sand dunes. *Physical Review E*, 66(3):031302, 2002.
- [16] Deguo Zhang, Clément Narteau, and Olivier Rozier. Morphodynamics of barchan and transverse dunes using a cellular automaton model. *Journal of Geophysical Research: Earth Surface*, 115(F3), 2010.
- [17] Orencio Durán, Veit Schwämmle, Pedro G Lind, and Hans J Herrmann. The dune size distribution and scaling relations of barchan dune fields. *Granular Matter*, 11(1):7–11, 2009.
- [18] Orencio Durán, Veit Schwämmle, Pedro G Lind, and Hans J Herrmann. Size distribution and structure of barchan dune fields. *Nonlinear Processes in Geophysics*, 18(4):455–467, 2011.
- [19] Hicham Elbelrhiti. Initiation and early development of barchan dunes: A case study of the moroccan atlantic sahara desert. *Geomorphology*, 138(1):181–188, 2012.
- [20] Stacey L Worman, A Brad Murray, Ryan Littlewood, Bruno Andreotti, and Philippe Claudin. Modeling emergent large-scale structures of barchan dune fields. *Geology*, 41(10):1059–1062, 2013.
- [21] Willian Righi Assis and Erick de Moraes Franklin. A comprehensive picture for binary interactions of subaqueous barchans. *Geophysical Research Letters*, 47(18):e2020GL089464, 2020.
- [22] Serina Diniega, Karl Glasner, and Shane Byrne. Long-time evolution of models of aeolian sand dune fields: Influence of dune formation and collision. *Geomorphology*, 121(1-2):55–68, 2010.
- [23] Mathieu Génois, Pascal Hersen, Sylvain Courrech Du Pont, and Guillaume Grégoire. Spatial structuring and size selection as collective behaviours in an agent-based model for barchan fields. *The European Physical Journal B*, 86(11):1–13, 2013.
- [24] Atsunari Katsuki, Macoto Kikuchi, Hiraku Nishimori, Noritaka Endo, and Keisuke Taniguchi. Cellular model for sand dunes with saltation, avalanche and strong erosion: collisional simulation of barchans. *Earth Surface Processes and Landforms*, 36(3):372–382, 2011.
- [25] Karol A Bacik, Sean Lovett, P Caulfield Colm-cille, and Nathalie M Vriend. Wake induced long range repulsion of aqueous dunes. *Physical review letters*, 124(5):054501, 2020.
- [26] Noritaka Endo, Keisuke Taniguchi, and Atsunari Katsuki. Observation of the whole process of interaction between barchans by flume experiments. *Geophysical Research Letters*, 31(12), 2004.
- [27] Dominic T Robson, Andreas CW Baas, and Alessia Annibale. A combined model of aggregation, fragmentation, and exchange processes: insights from analytical calculations. *Journal of Statistical Mechanics: Theory and Experiment*, 2021(5):053203, 2021.
- [28] Hicham Elbelrhiti, Philippe Claudin, and Bruno Andreotti. Field evidence for surface-wave-induced instability of sand dunes. *Nature*, 437(7059):720–723, 2005.
- [29] Pieter Vermeesch. Solitary wave behavior in sand dunes observed from space. *Geophysical Research Letters*, 38(22), 2011.

- [30] Veit Schwämmle and Hans J Herrmann. Solitary wave behaviour of sand dunes. *Nature*, 426(6967):619–620, 2003.
- [31] AR Lima, G Sauermaun, HJ Herrmann, and K Kroy. Modelling a dune field. *Physica A: Statistical Mechanics and its Applications*, 310(3-4):487–500, 2002.
- [32] Marc Mézard and Giorgio Parisi. The bethe lattice spin glass revisited. *The European Physical Journal B-Condensed Matter and Complex Systems*, 20(2):217–233, 2001.
- [33] Elena Agliari, Alessia Annibale, Adriano Barra, ACC Coolen, and Daniele Tantari. Immune networks: multitasking capabilities near saturation. *Journal of Physics A: Mathematical and Theoretical*, 46(41):415003, 2013.
- [34] Pavel L Krapivsky, Sidney Redner, and Eli Ben-Naim. *A kinetic view of statistical physics*. Cambridge University Press, 2010.
- [35] Pascal Hersen. Flow effects on the morphology and dynamics of aeolian and subaqueous barchan dunes. *Journal of Geophysical Research: Earth Surface*, 110(F4), 2005.
- [36] Erick de Moraes Franklin and François Charru. Subaqueous barchan dunes in turbulent shear flow. part 1. dune motion. *Journal of Fluid Mechanics*, 675:199, 2011.
- [37] Eric JR Parteli, Orencio Duran, and Hans J Herrmann. Minimal size of a barchan dune. *Physical Review E*, 75(1):011301, 2007.
- [38] Pauli Virtanen, Ralf Gommers, Travis E. Oliphant, Matt Haberland, Tyler Reddy, David Cournapeau, Evgeni Burovski, Pearu Peterson, Warren Weckesser, Jonathan Bright, Stéfan J. van der Walt, Matthew Brett, Joshua Wilson, K. Jarrod Millman, Nikolay Mayorov, Andrew R. J. Nelson, Eric Jones, Robert Kern, Eric Larson, C J Carey, İlhan Polat, Yu Feng, Eric W. Moore, Jake VanderPlas, Denis Laxalde, Josef Perktold, Robert Cimrman, Ian Henriksen, E. A. Quintero, Charles R. Harris, Anne M. Archibald, Antônio H. Ribeiro, Fabian Pedregosa, Paul van Mulbregt, and SciPy 1.0 Contributors. SciPy 1.0: Fundamental Algorithms for Scientific Computing in Python. *Nature Methods*, 17:261–272, 2020.
- [39] Constantino Tsallis. Possible generalization of boltzmann-gibbs statistics. *Journal of statistical physics*, 52(1):479–487, 1988.
- [40] Constantino Tsallis and Daniel A Stariolo. Generalized simulated annealing. *Physica A: Statistical Mechanics and its Applications*, 233(1-2):395–406, 1996.
- [41] Y Xiang, DY Sun, W Fan, and XG Gong. Generalized simulated annealing algorithm and its application to the thomson model. *Physics Letters A*, 233(3):216–220, 1997.
- [42] Y Xiang and XG Gong. Efficiency of generalized simulated annealing. *Physical Review E*, 62(3):4473, 2000.
- [43] Yang Xiang, Sylvain Gubian, Brian Suomela, and Julia Hoeng. Generalized simulated annealing for global optimization: the gensa package. *R J.*, 5(1):13, 2013.
- [44] O Durán, V Schwämmle, and H Herrmann. Breeding and solitary wave behavior of dunes. *Physical Review E*, 72(2):021308, 2005.